Journal of Electrical Engineering, Vol. 74, No. 3, 2023, pp. 218-227

sciendo

PAPER

Analysis of porous silicon structures using FTIR and Raman spectroscopy

Martin Králik[1], Martin Kopani[2]

This work deals with the production of porous silicon samples by electrochemical etching method and their analysis using FTIR and Raman spectroscopy. Porous silicon samples were prepared under various conditions, such as etching time and current density. A p-type silicon substrate was used to prepare the porous silicon structures. FTIR spectroscopy was performed to determine the chemical bonds formed during the etching process. The structural properties of the prepared samples were investigated by Raman spectroscopy.

Keywords: electrochemical etching, FTIR spectroscopy, Raman spectroscopy, porous silicon

1. Introduction

Porous silicon (pSi) is a material with a wide range of industrial applications, an example is its use in next-generation lithium–ion (Li-Ion) batteries, as well as applications in the fields of biomedicine, photovoltaics, optoelectronics and sensors. The advantage of pSi is its simple and low-cost production. There are several ways to produce pSi, with electrochemical etching being the most commonly used technology.

In the case of next-generation Li-Ion batteries, pSi is used as an alternative anode material to graphite, as it achieves more than ten times the theoretical gravimetric specific capacity value (~4200 mA h g^{-1}). In the field of biomedicine, pSi may find its application in the production of biosensors because of one of its significant properties, namely light emission in the visible region of the spectrum. Further application of pSi in the field of biomedicine is, for example, disease diagnosis and targeted supply of medicinal products to the body, as targeted and localized release of therapeutic substances can be ensured, [1–3]. As for photovoltaic applications pSi, it can be described as one of the highly promising structures in this area. The advantage of pSi is mainly its low spectral reflectivity in the relevant area of the electromagnetic spectrum (~ from 300 to 1000 nm), where its spectral reflectivity is below 2.5 %.

Currently, there are several methods of pSi production, among the most common methods it is possible to include electrochemical etching, metal assisted chemical etching and plasma etching. In the case of applications of porous silicon in the field of photovoltaics, the use of the metal assisted chemical etching method is not desirable since after the production process it is not possible to remove all metal residues from the porous structure, which could have a negative impact on the properties of the solar cell. Plasma etching has an advantage over the above methods in the absence of toxic substances in the production process, and another advantage is the ability to easily control the size and shape of the porous structure. However, plasma etching is a very expensive method. At present it is possible to designate as the most used method of pSi electrochemical etching production, due to the simplicity of this method.

Porous silicon can be divided into three categories based on the classification of porous materials as a function of their pore size dp (IUPAC) by the International Union of Pure and Applied Chemistry: microporous silicon μpSi (dp < 2 nm), mesoporous silicon 6 mpSi (2 nm < dp < 50 nm) and macroporous silicon MpSi (dp > 50 nm). Based on morphological details, pSi can be categorized as sponge pSi (μpSi and mpSi), pSi with cylindrical pores with rough or smooth walls (MpSi). The size and shape of the porous structure may be affected by the technological process of production [4–6].

The following recommendations generally apply to the production of microporous silicon: the use of a lightly doped p-type silicon substrate, the low current density in the etching process and the use of highly concentrated HF (> 40 %) [20–21], [24]. Based on the published experiments, the microporous silicon can be prepared on the using the electrochemical etching of a silicon substrate p-type doped with boron (ρ = 0.5 Ωcm) in a solution of 49 % HF and ethanol in a ratio of 1:1 at a current density of 30 $mAcm^{-2}$ and an etching time of 10 minutes [5].

Mesoporous silicon can be prepared by electrochemical etching of a highly doped silicon substrate of p-type, or n-type (p^+-type, p^{++}-type, n^+-type, n^{++}-type). The resistivity of p^{++}-type silicon is approximately 1 mΩcm. The result of electrochemical etching of

[1] Institute of Aurel Stodola, Faculty of Electrical Engineering and Information Technology, University of Zilina, Komenskeho 843, 031 01 Liptovsky Mikulas, Slovakia
[2] Institute of Medical Physics, Biophysics, Informatics and Telemedicine, Faculty of Medicine, Comenius University, Sasinkova 4, 811 08, Bratislava, Slovakia
martin.kralik@feit.uniza.sk

https://doi.org/10.2478/jee-2023-0028, Print (till 2015) ISSN 1335-3632, On-line ISSN 1339-309X

the silicon substrate p^{++}-type is a smaller number of pores with a larger diameter. The diameter of the pores can also be controlled by means of current density. Based on published experiments, mesoporous silicon can be prepared by electrochemical etching of p-type silicon (ρ = 0.001 Ωcm) in a solution of 48 % HF and ethanol in a ratio of 3:1 (HF/ethanol) at a current density of 200 $mAcm^{-2}$ and etching time of 30 seconds. The result of this process is the formation of a porous structure with a thickness of several nm, which is subsequently removed using sodium hydroxide (NaOH) solution. After removal of this porous layer, the electrochemical etching process is continued in a solution of 48 % HF and ethanol in a ratio of 3:1 (HF/ethanol) at a current density of 420 $mAcm^{-2}$ for 60 seconds. The result of this experiment is a ~12 μm porous structure with a pore diameter of ~50 nm and a porosity of ~75% [5].

Macroporous silicon can be prepared by electrochemical etching of a silicon substrate of n-type, or p-type. In the case of electrochemical etching of the n-type silicon substrate, it is necessary to illuminate the front or back side of silicon substrate during the etching process. The silicon dissolving process and the associated pore formation are initiated by holes that are minority charge carriers in the n-type silicon substrate. The illumination of the silicon substrate during the etching process ensures the holes generation and subsequent the formation of the macroporous structure [6].

2. Experiment

Figure 1 shows the basic scheme of the electrochemical etching method that was used to prepare the pSi samples published in this work. The basic components of this system are a platinum electrode, an etching cell, a rear electrode and an o-ring. The platinum electrode is used due to its high chemical resistance. The etching cell is made of Teflon (PTFE), which is one of the most chemically resistant material to hydrofluoric acid (HF). The o-ring serves as a seal to minimize the risk of unwanted leakage of the HF solution. Among the most recommended materials for o-rings are perfluoroelastomeric compounds (FFKM) due to their high thermal and chemical resistance. The back electrode is used to create ohmic contact on the back of the silicon substrate. In the case of p-type silicon substrate, the use of an aluminum electrode is recommended and in the case of n-type silicon substrate, the use of the Au–Sb electrode. The use of the back electrode is generally required for lightly doped silicon (< 10^{18} cm^{-3}) [4–7].

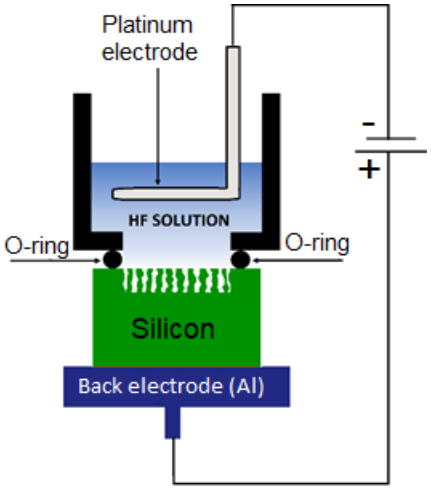

Fig. 1. Schematic diagram of electrochemical etching.

Boron-doped p-type silicon wafers with orientation 100, resistivity 0.0010 – 0.0015 Ωcm, and a thickness of 525 ± 15 μm were used to produce pSi samples published in this work. The front of the silicon wafers was polished and the surface of the back was chemically etched. The back surface of the silicon wafers consisted of a 500 nm oxide layer that was removed by immersion of wafers in the 49% HF solution for 10 seconds.. Porous structures were prepared by the electrochemical etching of silicon wafers in a solution of 49% HF and 99.8% ethanol in a ratio of 3 (HF) : 1 (ethanol). The samples were prepared under different conditions, such as etching time and current density. The parameters of the technological process are listed in the Tab. 1.

Table 1 Parameters used in the production process of pSi samples

Samples	Etching time (min)	Current density (mAcm^{-2})	Current (mA)
S1	10	19.7	50
S2	15	19.7	50
S3	10	31.4	80
S4	15	31.4	80

3. Results and discussion

This part of the work deals with the analysis of experimental data obtained from FTIR and Raman spectroscopy. FTIR spectroscopy was performed to identify chemical bonds created in the pSi samples. Identification of chemical bonds formed in pSi is necessary for correct analysis of the optical properties of pSi structures. The analysis of optical properties includes the selection of a suitable dispersion model and its optimization in order to determine the optical parameters such as refractive index, extinction coefficient and optical bandwidth. Raman spectroscopy is mainly used to analyze the structural properties of pSi structures, such as porosity and tensile stress.

3.1 FTIR spectroscopy

In order to identify the chemical bonds formed during the etching process, experimental absorbance measurements in the 600 cm^{-1} to 3300 cm^{-1} spectral region of prepared pSi samples were performed. Experimental measurements were performed using a Nicolet™ iS™ 10 FTIR spectrometer. Experimental data of the absorbance obtained from FTIR spectroscopy and identification of the absorption peaks are shown in Fig. 2. Baseline correction of the FTIR spectra was performed before absorption peaks analysis. FTIR absorption spectra of prepared pSi samples after baseline correction are shown in Fig. 3.

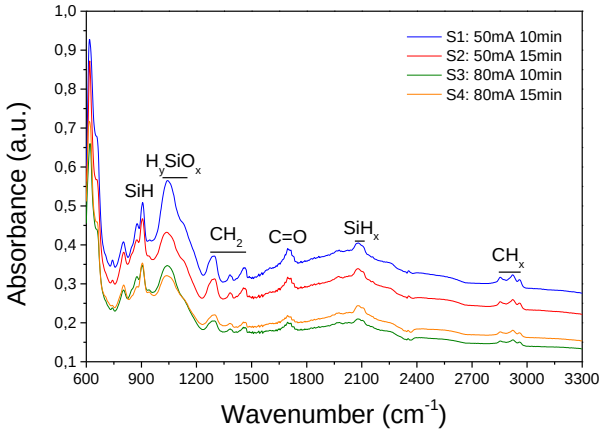

Fig. 2. FTIR absorption spectra.

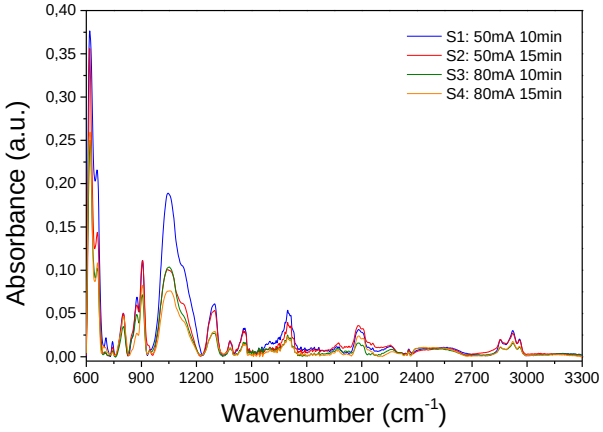

Fig. 3. FTIR absorption spectra after baseline correction.

Figure 4 shows the absorbance FTIR spectra of the samples S1, S2, S3 and S4 in the 2840 cm^{-1} to 2980 cm^{-1} spectral region and multiple peak-fitting of absorption peaks. The absorption peaks located in the 2840–2980 cm^{-1} spectral region are specific for CH_x bonds. Multiple peak–fitting were realized using the five Gaussian functions. The symmetric CH_2 stretching vibration ca be observed at ~2853 cm^{-1}, symmetric CH_3 stretching vibration at ~2878 cm^{-1}, antisymmetric CH_2 stretching vibration at ~2923 cm^{-1} and antisymmetric CH_3 stretching vibration at 2959 cm^{-1}. The position of the absorption peaks and identification of CH_x bonds in the spectral range from 2840 to 2980 cm^{-1} are listed in Tab.2. Identification of CH_x bonds was performed on the basis of the results published in [8].

Table 2 Identification of the absorption peaks in the spectral range from 2840 to 2980 cm^{-1}

Samples	Symmetric CH_2 stretching (cm^{-1})	Symmetric CH_3 stretching (cm^{-1})	Antisymmetric CH_2 stretching (cm^{-1})	Antisymmetric CH_3 stretching (cm^{-1})
S1	2853.4	2877.6	2922.3	2959.5
S2	2853.2	2878.1	2922.5	2959.2
S3	2854.0	2878.4	2922.9	2959.9
S4	2852.9	2877.1	2922.6	2959.3

A significant decrease in the intensity of the absorption peaks specific for CH_x bonds is observed with increasing current density during etching process. A decrease in intensity of absorption peaks is also observed with increasing etching time, but this decrease in intensity is not as significant as in the case of increasing current density. The CH_x bonds in pSi samples come from ethanol, which is part of the etching solution.

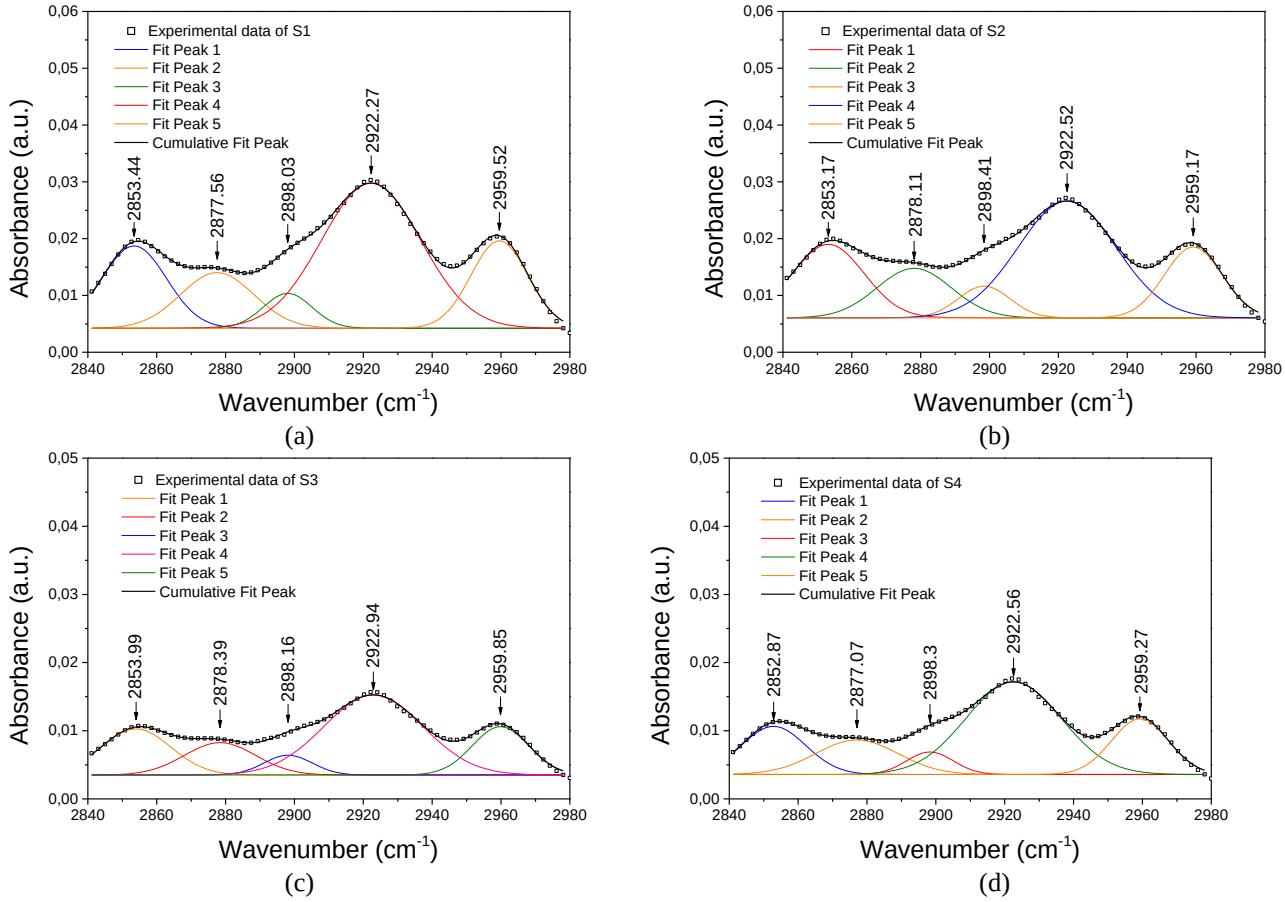

Fig. 4. FTIR absorption spectra in the 2840 cm^{-1} to 2980 cm^{-1} spectral region and multiple peak–fitting of absorption peaks.

Figure 5 shows the absorbance FTIR spectra of the samples S1, S2, S3 and S4 in the 2050 cm^{-1} to 2150 cm^{-1} spectral region and multiple peak–fitting of absorption peaks. The absorption peaks located in the 2050–2150 cm^{-1} spectral region are specific for SiH_x bonds. Multiple peak–fitting were realized using the three Gaussian functions.

The above spectral region consists of three absorption peaks at ~2081 cm^{-1}, ~2110 cm^{-1} and ~2141 cm^{-1}, which are specific for SiH, SiH_2 and SiH_3 bonds. The SiH stretching vibration can be observed at ~2081 cm^{-1}, SiH_2 stretching vibration at ~2110 cm^{-1} and SiH_3 stretching vibration at 2141 cm^{-1}. The absorption peaks position and identification of SiH_x bonds in the spectral range from 2050 to 2150 cm^{-1} are listed in Tab. 3. Identification of SiH_x bonds was performed on the basis of the results published in [9–10].

Table 3 Identification of the absorption peaks in the spectral range from 2050 to 2150 cm^{-1}

Samples	SiH stretching (cm^{-1})	SiH_2 stretching (cm^{-1})	SiH_3 stretching (cm^{-1})
S1	2080.6	2110.4	2140.4
S2	2081.4	2110.2	2141.3
S3	2080.8	2109.2	2138.9
S4	2080.4	2110.1	2140.2

The formation of SiH_x bonds is with high probability caused by the release of hydrogen gas during the etching process. In the case of samples S1 and S2, a decrease in the intensity of absorption peaks in the SiH_x region was observed with an increase in etching time. In the case of samples S3 and S4, an increase in the intensity of the absorption peaks was observed with increasing etching time.

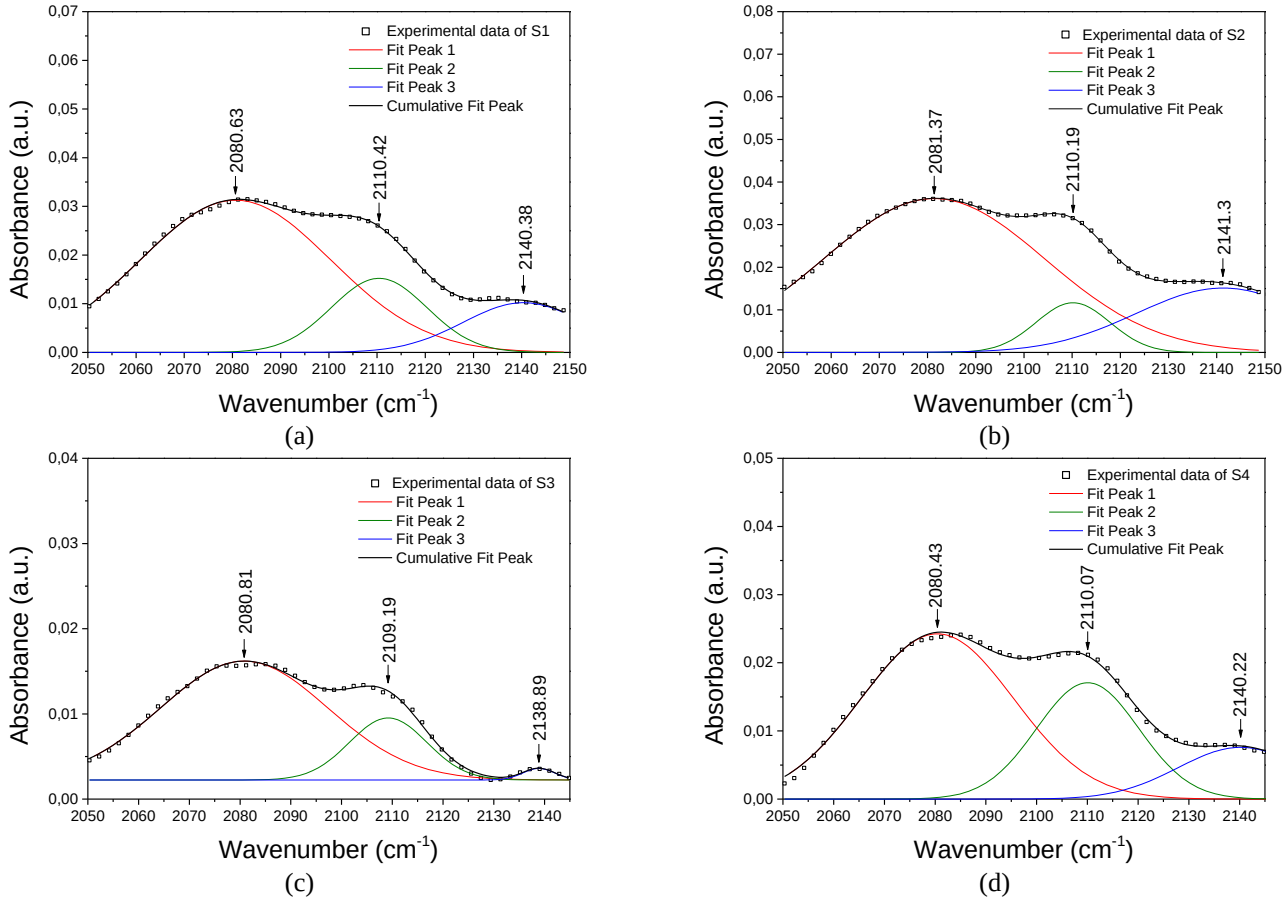

Fig. 5. FTIR absorption spectra in the 2050 cm^{-1} to 2150 cm^{-1} spectral region and multiple peak–fitting of absorption peaks.

Figure 6 shows the absorbance FTIR spectra of the samples S1, S2, S3 and S4 in the 960 cm^{-1} to 1240 cm^{-1} spectral region and multiple peak–fitting of absorption peaks. Multiple peak-fitting were realized using the three (four in the case of sample S4) Gaussian functions. The absorption peaks position in the spectral range from 960 to 1240 cm^{-1} and its identification are listed in Tab. 4. The identification of absorption peaks (~1030 cm^{-1}, ~1120 cm^{-1}) was realized on the basis of the results published in the work of M. Kopani *et al* [12].

Table 4 Identification of the absorption peaks in the spectral range from 960 to 1230 cm^{-1}

Samples	H_ySiO_x complexes (cm^{-1})	Si–O stretching (cm^{-1}) [10]	H_ySiO_x complexes (cm^{-1})
S1	1037.4	1074	1123.3
S2	1025.8	1067.6	1125
S3	1034.2	1072.8	1117.9
S4	1030.3	1070.6	1117.8

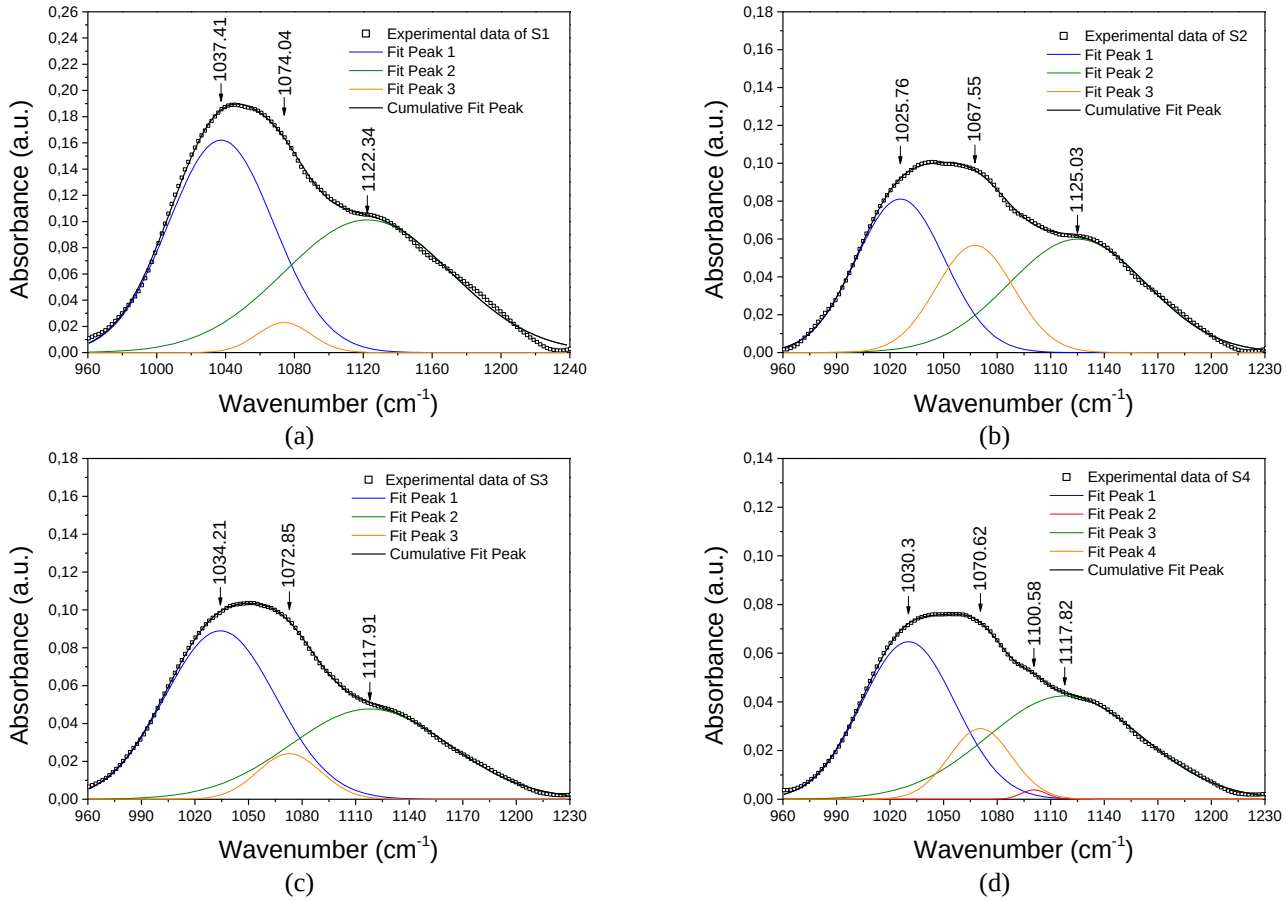

Fig. 6. FTIR absorption spectra in the 960 cm^{-1} to 1230 cm^{-1} spectral region and multiple peak–fitting of absorption peaks.

Figure 7 shows the absorbance FTIR spectra of the samples S1, S2, S3 and S4 in the 600 cm^{-1} to 690 cm^{-1} spectral region and multiple peak-fitting of absorption peaks. Multiple peak–fitting were realized using the two Gaussian functions. The absorption peaks position and its identification in the spectral range from 600 to 690 cm^{-1} are listed in Tab. 5. The peaks identification presented in the Tab. 5 were obtained based on the results of work published by Y.Ogata *et al* [10].

Table 5 Identification of the absorption peaks in the spectral range from 600 to 690 cm^{-1}.

Samples	SiH bending (cm^{-1})	SiH_2 wagging (cm^{-1})
S1	617.3	660.9
S2	617.9	660.4
S3	619.6	659.9
S4	618.9	662.7

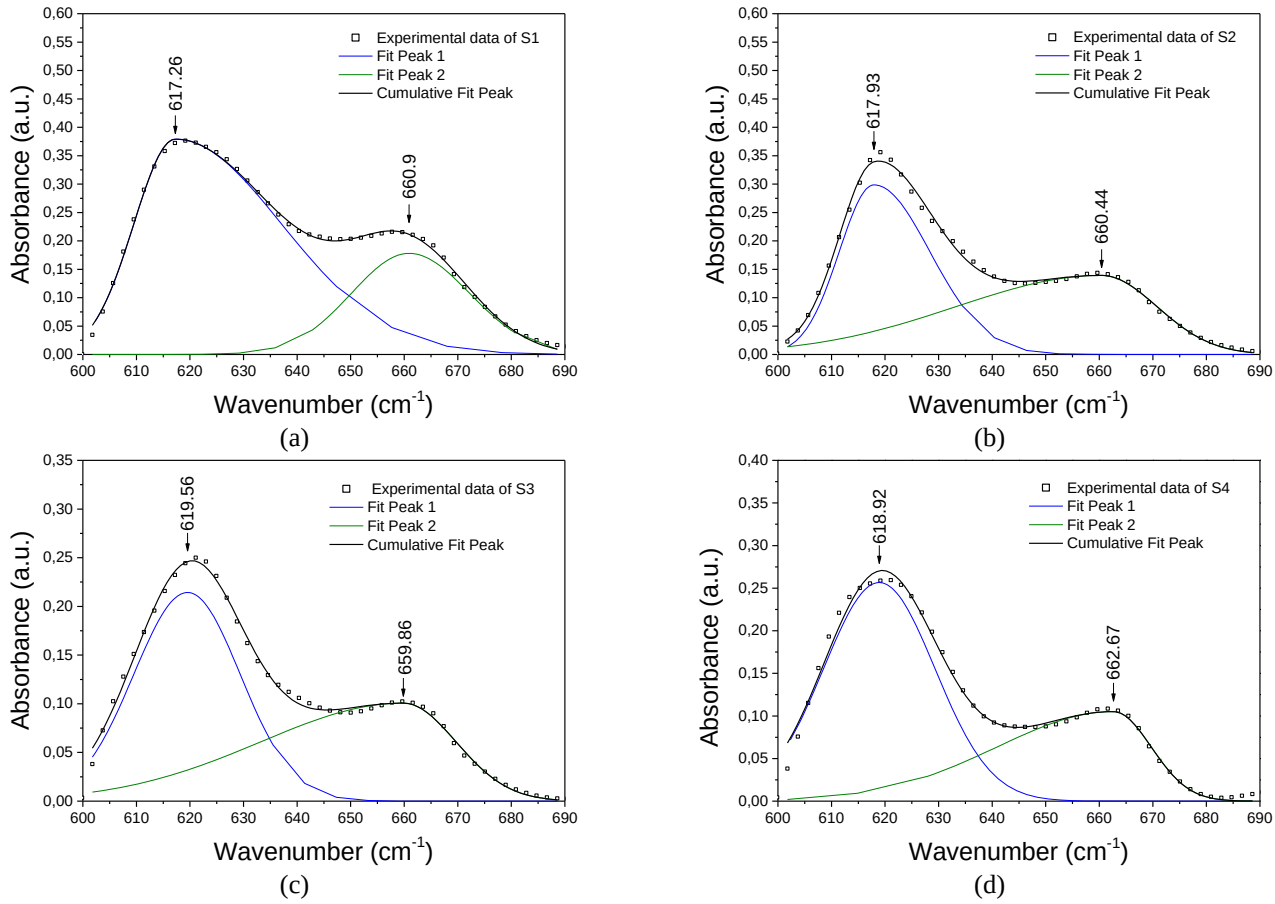

Fig. 7. FTIR absorption spectra in the 600 cm^{-1} to 690 cm^{-1} spectral region and multiple peak–fitting of absorption peaks.

Figure 8 shows the absorbance FTIR spectra of the samples S1, S2, S3 and S4 in the 830 cm^{-1} to 930 cm^{-1} spectral region and multiple peak–fitting of absorption peaks. Multiple peak–fitting were realized using the three Gaussian functions. The identification of absorption is listed in Tab. 6 and was realized on the basis of the results published in the work of M.Kopani *et al* [12].

Table 6 Identification of the absorption peaks in the spectral range from 830 to 930 cm^{-1}

Samples	H_ySiO_x complexes (cm^{-1})	SiH_3 (cm^{-1})	SiH (cm^{-1})
S1	846.8	874.8	906.2
S2	849.2	873.4	905.5
S3	847.6	874.1	904.5
S4	851.8	873.6	904.7

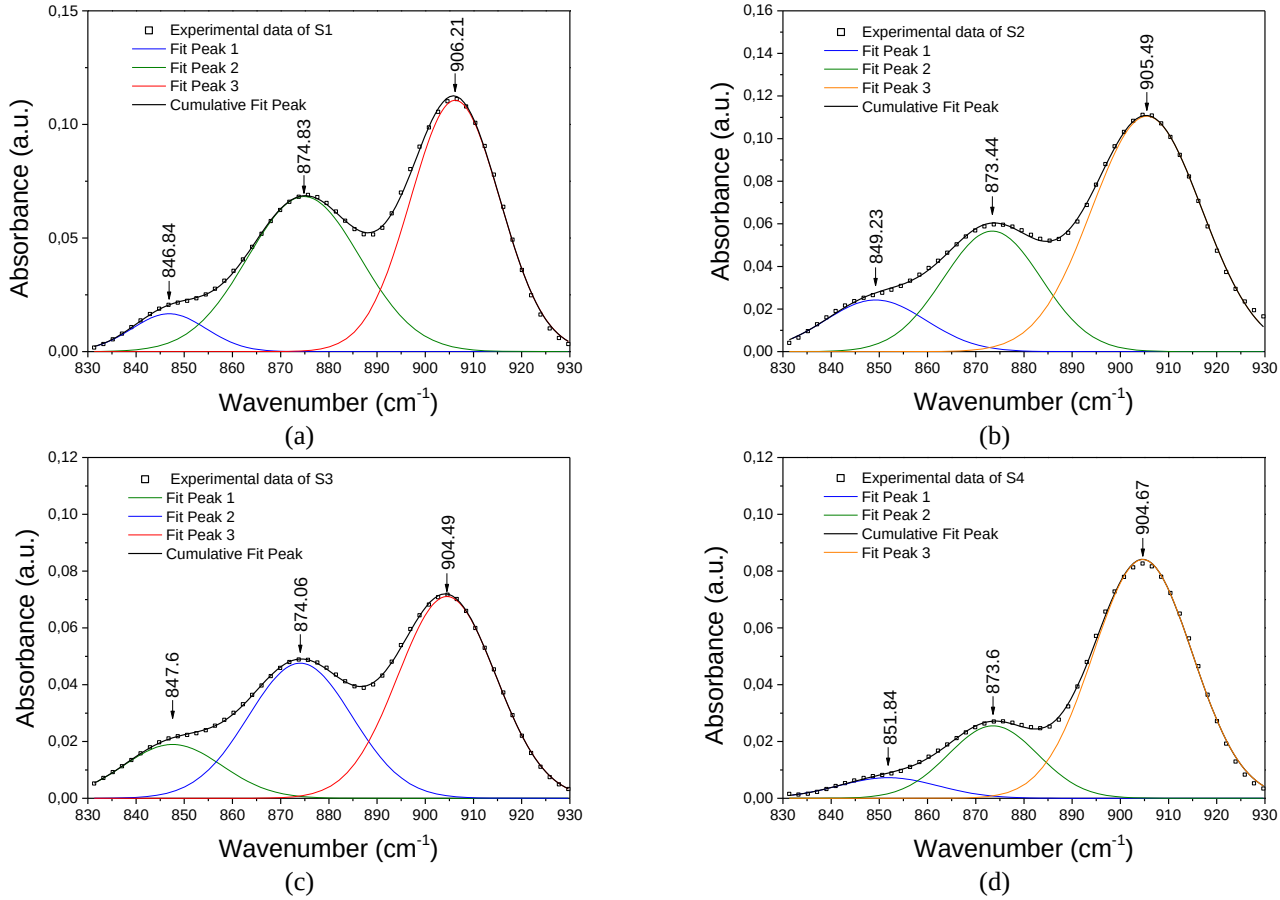

Fig. 8. FTIR absorption spectra in the 830 cm^{-1} to 930 cm^{-1} spectral region and multiple peak–fitting of absorption peaks.

3.2 Raman spectroscopy

Raman spectroscopy is one possible way to analyze structural properties of porous silicon structures. In investigating the structural properties of prepared samples, we focused on the first–order Raman profile, which is located in the region of ~ 520 cm^{-1}. Figure 9 shows the Raman spectra of the prepared samples in the 300 cm^{-1} to 1100 cm^{-1} spectral region. First-order Raman profile is significantly affected by the etching time and current density.

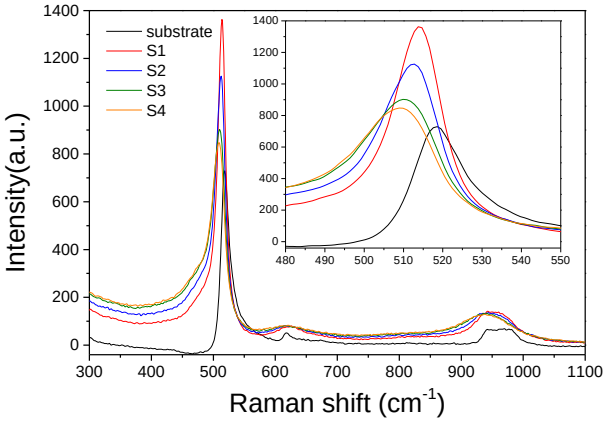

Fig. 9. Raman scattering spectra.

In the case of the first–order Raman profile, two parameters were analyzed, namely the peak position and its intensity. From the experimental data of Raman spectroscopy, a red–shift (compared to c-Si: 520 cm^{-1}) and change in peak intensity of the Raman

profile can be observed. Based on the change in the peak position of the first–order Raman profile, the average size of the crystallite and the tensile stress can be determined by the following relations [14]

$$D=2\pi(B/\Delta\omega)^{0.5}, \quad (1)$$

$$TS=-250\Delta\omega, \quad (2)$$

where D is the average size of the crystallite (nm), B is constant (2.21 nm^2cm^{-1}), TS is biaxial tensile stress (MPa) and $\Delta\omega$ is shift of central 1st order Raman profile position of the etched silicon layer compared to c-Si. Peak fitting of the 1st order Raman profile in the 490 cm^{-1} to 530 cm^{-1} spectral region was performed in order to determine the $\Delta\omega$ and TS values. The calculated values of average size of the crystallite and is biaxial tensile stress are listed in Tab. 7. The increase in etching time and current density in addition to the red–shift also significantly reduced the peak intensity of the 1st order Raman profile. The results of the work published by F. Zhong *et al* [14] suggest that decrease in the peak intensity of the 1st order Raman profile can by caused by reduction of SiH_x bonds. These considerations are also confirmed by the results of experimental measurements of FTIR spectroscopy.

Table 7 Parameters of the first–order Raman profile

Samples	Raman shift (cm^{-1})	TS (MPa)	D (nm)
S1	514.6	1357.5	2.6
S2	513	1747.5	2.0
S3	511.2	2205	1.6
S4	510	2500	1.4

With increasing of etching time and current density the values of the biaxial tensile stress increase, which is caused by deformation of crystal lattice during the substrate etching. As the etching time and current density increase, it is also possible to observe a decrease in average size of the crystallite.

4 Conclusion

In this work, studies and analyzes of porous silicon structures produced by electrochemical etching were presented. Porous silicon structures were prepared under various conditions, such as etching time and current density. The porous silicon structures were investigated by FTIR and Raman spectroscopy.

FTIR spectroscopy is the first step in analyzing the optical properties of porous silicon structures. Experimental data obtained from FTIR spectroscopy indicate a significant concentration of SiH_x and CH_x bonds in the prepared samples. There is also a significant concentration of H_ySiO_x complexes in the prepared samples. The intensity of the absorption peaks of above bonds and complexes decreases with increasing etching time and current density. The identification of the formed chemical bonds in the prepared samples can provide a basis for the construction of a suitable theoretical model describing the refractive index dispersion.

Raman spectroscopy provided information about the structural properties of the prepared samples. First-order Raman profile analysis provided information about average size of the crystallite and deformation of crystal lattice during the substrate etching. Calculations of biaxial tensile stress and average size of the crystallite were based on the shift of the 1st order Raman profile.

Acknowledgement

The work was supported grant of Science and Technology Assistance Agency APVV–15–0152, Scientific Grant Agency of the Ministry of Education of Slovak Republic.

References

[1] T. Kumeria, S.J.P. McInnes, S.Maher, and A. Santos, "Porous silicon for drug delivery applications and theranostics: recent advances, critical review and perspectives", *Expert Opinion on Drug Delivery* 14 (2017) 1407–1422

[2] M. Perrone Donnorso et al., "Nanoporous silicon nanoparticles for drug delivery applications", *Microelectronic Engineering* 98 (2012) 626–629

[3] K.Tamarov et al., "Temperature responsive porous silicon nanoparticles for cancer therapy – spatiotemporal triggering through infrared and radiofrequency electromagnetic heating", *Journal of Controlled Release* 241 (2016) 220–228

[4] L. Volker, Electrochemistry of Silicon, Wiley–VCH Verlag GmbH ISBN 3–527–29321–3 (2002)

[5] M. J. Sailor, Porous Silicon in Practice, Wiley–VCH Verlag & Co. KGaA ISBN 978–3–527–64190–1 (2012)
[6] D. Losic, Electrochemically Engineered Nanoporous Materials, Springer International Publishing AG ISBN 978–3–319–20346–1 (2015)
[7] L. Canham, Handbook of Porous Silicon, Second Edition, Springer International Publishing AG, part of Springer Nature ISBN 978–3–319–71379–3 (2018) 13–24
[8] K. Herynková, M. Šlechta, P. Šimáková, A. Fučíková and O. Cibulka, "Agglomeration of luminescenct porous silicon nanoparticles in colloidal solutions", *Nanoscale Research Letters* 11 (2016) 1–5
[9] C. A. Caras, J. M. Reynard, R. E. Deuro and F. V. Bright, "Link Between O_2SiH Infrared Band Amplitude and Porous Silicon Photoluminescence During Ambient O_3 Oxidation", *Applied Spectroscopy* 66 (2012) 951–957
[10] Y. Ogata, H. Niki, T. Sakka and M. Iwasaki, "Hydrogen in Porous Silicon: Vibrational Analysis of SiH_x Species", *J. Electrochem. Soc.* 142 (1995) 195–201
[11] L. Canham, Handbook of Porous Silicon, Second Edition, Springer International Publishing AG, part of Springer Nature ISBN 978–3–319–71379–3 (2018) 705–712
[12] M Kopani et al., "Effect of etching time in hydrofluoric acid on the structure and morphology of n-type porous silicon", *Applied Surface Science* 532 (2020)
[13] Z.H. Wang, T. Urisu, H. Watanabe, K. Ooi, G.R. Rao, S. Nanbu, J. Maki, M. Aoyagi, "Assignment of surface IR absorption spectra observed in the oxidation reactions: 2H + HO/Si(100) and HO + H/Si(100)", *Surf. Sci.* 575 (2005) 330–342
[14] F. Zhong and Z.–Hong Jia, "Raman scattering study on pristine and oxidized n-type porous silicon", *Physica B: Condensed Matter* 441 (2013) 77–70

Received 21 February 2023